



Electrochemical hydriding and thermal dehydriding properties of nanostructured hydrogen storage MgNi26 alloy

V. KNOTEK¹, O. EKRT¹, M. LHOTKA², D. VOJTĚCH¹

1. Department of Metals and Corrosion Engineering, University of Chemistry and Technology Prague, Technická 5, 166 28 Prague 6, Czech Republic;

2. Department of Inorganic Technology, University of Chemistry and Technology Prague, Technická 5, 166 28 Prague 6, Czech Republic

Received 12 August 2015; accepted 29 January 2016

Abstract: The MgNi26 alloy was prepared by three different methods of gravity casting (GC), mechanical alloying (MA) and rapid solidification (RS). All samples were electrochemically hydrided in a 6 mol/L KOH solution at 80 °C for 240 min. The structures and phase compositions of the alloys were studied using optical microscopy and scanning electron microscopy, energy dispersive spectrometry and X-ray diffraction. A temperature-programmed desorption technique was used to measure the absorbed hydrogen and study the dehydriding process. The content of hydrogen absorbed by the MgNi26-MA (approximately 1.3%, mass fraction) was 30 times higher than that of the MgNi26-GC. The MgNi26-RS sample absorbed only 0.1% of hydrogen. The lowest temperature for hydrogen evolution was exhibited by the MgNi26-MA. Compared with pure commercial MgH₂, the decomposition temperature was reduced by more than 200 °C. The favourable phase and structural composition of the MgNi26-MA sample were the reasons for the best hydriding and dehydriding properties.

Key words: magnesium alloy; hydrogen storage; electrochemical hydriding; mechanical alloying; melt spinning

1 Introduction

In the last three decades, magnesium alloys have been extensively studied because magnesium has one of the largest hydrogen gravimetric densities. Magnesium is theoretically capable of absorbing up to 7.6% (mass fraction) of hydrogen in the form of MgH₂. In addition, magnesium is a very light structural material, and it is relatively inexpensive compared to other hydride-formers (Ti, Zr, V). However, pure MgH₂ suffers from high thermodynamic stability, which results in a decomposition temperature of more than 300 °C [1]. Such a high desorption temperature is impractical because of the unfavorable ratio of supplied to obtained energy. For this reason, many attempts have been made to destabilize magnesium hydride, including alloying with transition and rare-earth metals and adding catalysts [2]. Another approach is to produce nano-crystalline or amorphous structures, such as ball milling, rapid solidification and other techniques [3–5]. The nanostructuring of Mg is beneficial because it produces

high concentrations of lattice defects, grain boundaries and interfaces, which are also good pathways for the diffusion of hydrogen.

Nickel has been known for a long time to enhance the magnesium hydriding/dehydriding properties [6]. Mg–Ni-based alloys subjected to nanoscaling exhibit excellent hydriding parameters during the gas hydriding process [7]. The presence of nickel in Mg-based alloys also positively affects the hydrogen absorption during the electrochemical hydriding. In this case, however, nickel does not need to dissociate molecule of hydrogen, because electrochemical hydriding generates atomic hydrogen that can penetrate the material and produce hydrides.

In our previous study of the electrochemical hydriding of Mg-based alloys, we have shown that the as-cast MgNi26 alloy is the most promising alloy to absorb large amounts of hydrogen during electrochemical hydriding [8]. Therefore, in this work, we prepared the MgNi26 alloy by advanced methods of nanostructuring and evaluated the electrochemical hydriding and thermal dehydriding. Based on the results,

we discussed the contribution of the nanostructuring of MgNi26 alloy.

2 Experimental

To determine the influence of microstructure on electrochemical hydriding, the MgNi26 alloy (mass fraction, %) was prepared by three different methods. The first method was classical gravity casting (GC), in which an ingot of MgNi26 was prepared by the induction melting of pure Mg and Ni (99.9% purity) under a protective atmosphere of argon. The ingot was 100 mm in length and 30 mm in diameter. The second method was mechanical alloying (MA). In this case, commercial powders of Mg (Sigma Aldrich, <44 μm , 99.8%) and Ni (Merck, <10 μm , 99.9%) were subjected to mechanical milling in a planetary ball mill (Retsch PM 100) for 240 min under an argon protective atmosphere. The mass ratio of powder to ball was 1:100. The milling time was selected as a sufficient time to achieve the formation of the Mg_2Ni phase from all of the initial nickel. The last method of MgNi26 alloy preparation was rapid solidification (RS), namely melt spinning. A part of an as-cast ingot of MgNi26 alloy was used for this purpose. The alloy was remelted and rapidly solidified on a rotating copper wheel under an argon atmosphere. The speed of the copper wheel was 40 m/s, and the thickness of the obtained ribbons was approximately 60 μm .

For electrochemical hydriding, the as-cast ingot was cut into a 1 mm-thick sample. Before hydriding, the surface of the sample was mechanically treated by grinding and polishing. The powder of MgNi26-MA was uniaxially cold-pressed into pellets at 750 MPa. Each pellet weighed 0.5 g and had a diameter of 1.6 cm and a length of 1 mm. The rapidly solidified ribbons were used as prepared. Electrochemical hydriding was conducted in a 6 mol/L KOH solution at 80 °C. The samples were immersed in an electrolyte, connected to a DC source and polarized as the cathode. A platinum wire was used as the anode. The current density during hydriding was 100 A/m^2 for all of the hydrided samples. The hydriding was performed for 240 min.

The microstructures of the MgNi26-GC, MgNi26-MA and MgNi26-RS samples were observed by optical microscopy (OM) and scanning electron microscopy (SEM, TESCAN Vega 3–LMU) and energy dispersive spectrometry (EDS, OXFORD INSTRUMENT Inca 350). The phase compositions of the samples both before and after hydriding were determined by X-ray diffraction (XRD, X Pert Pro, Cu K_α radiation). The hydrogen content in the hydrided bulk GC sample was determined using a glow discharge spectrometer (GDS, HORIBA JOBINYVON GD Profiler 2). Because the hydriding was performed in a strong alkaline bath, the formation of

a surface layer of magnesium hydroxide could be expected. To minimize the influence of this layer on the detection of hydrogen in the form of hydrides, oxygen was also analyzed to determine the position of the hydroxide/metal interface. The GDS analyzer was calibrated with respect to MgH_2 . In the case of the hydrided MgNi26-GC, MgNi26-MA and MgNi26-RS samples, both the hydrogen content and the temperatures of hydrogen evolution were determined via the temperature-programmed desorption technique (TPD, MICROMETRICS AutoChem II 2920). In addition to the hydrided samples, we also investigated the behavior of pure MgH_2 powder (20 μm , 98%, HiChem) under the same conditions. The desorption analysis was carried out in a reactor by heating under temperature-programmed control from ambient temperature to 673 K at a heating rate of 4 K/min using argon (50 mL/min). The gas stream leaving the reactor was passed through a water-vapor trap at 210 K, and the evolution of the hydrogen was detected using a thermal conductivity detector. The system was calibrated by a mixture of hydrogen with argon.

3 Results and discussion

3.1 Structures of samples

The microstructures of the MgNi26-GC alloy obtained by optical microscopy and scanning electron microscopy are shown in Fig. 1.

Since the eutectic point of the Mg–Ni alloys corresponds to 23.5% Ni (mass fraction) [9], the structure of the MgNi26-GC alloy (Fig. 1(a)) is dominated by a eutectic mixture of $\alpha\text{-Mg} + \text{Mg}_2\text{Ni}$. The eutectic mixture is very fine, as seen in Fig. 1(b), and contains a high fraction of interphase boundaries, which can serve as an efficient pathway for rapid hydrogen diffusion.

In Fig. 2, there is XRD pattern illustrating the phase composition of the MgNi26-GC sample. XRD pattern of the MgNi26-GC alloy confirms the presence of two eutectic phases: Mg and Mg_2Ni , as also seen in Fig. 1(b).

The typical deformed morphology of the MgNi26 powder sample obtained by mechanical alloying is presented in Fig. 3. The phase composition corresponds to that of the MgNi26-GC alloy. Only Mg and Mg_2Ni phases were detected.

The size of the particles in the MA sample is in the range of 0.5–40 μm . The larger particles correspond predominately to Mg because of its plasticity. These particles of Mg are covered with fine particles of the Mg_2Ni phase, which is more brittle than Mg. The Mg_2Ni phase has been known for a long time for its better thermodynamic ability to absorb hydrogen compared to Mg. On the other hand, Mg is theoretically able to

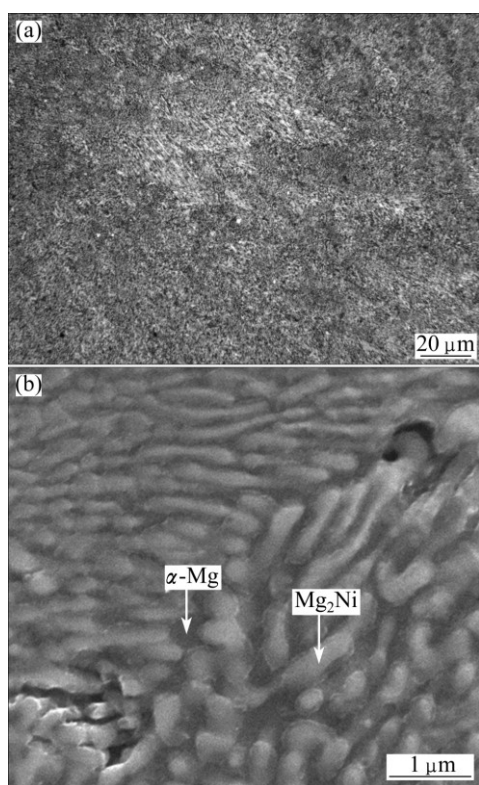


Fig. 1 Microstructures of MgNi26-GC alloy obtained by OM (a) and SEM (b)

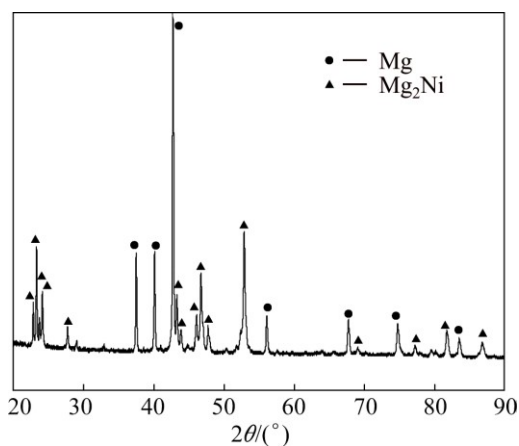


Fig. 2 XRD pattern of MgNi26-GC sample

absorb more than twice amount of hydrogen than Mg_2Ni . Therefore, the close connection of fine Mg_2Ni with Mg could be a promising factor to obtain rapid hydriding and a high amount of absorbed hydrogen simultaneously. The section of the cold-pressed MgNi26-MA sample is presented in Fig. 4. The porosity of the pellet is 29.1%. It is evident that the fine particles of MgNi26-MA powder create larger aggregates after uniaxial cold-pressing (Fig. 4(a)). However, the substructure of the aggregates can be observed in the detailed view (Fig. 4(b)). X-ray elemental maps of the cold-pressed pellet in Fig. 5 show a homogenous distribution of Mg and Ni. This

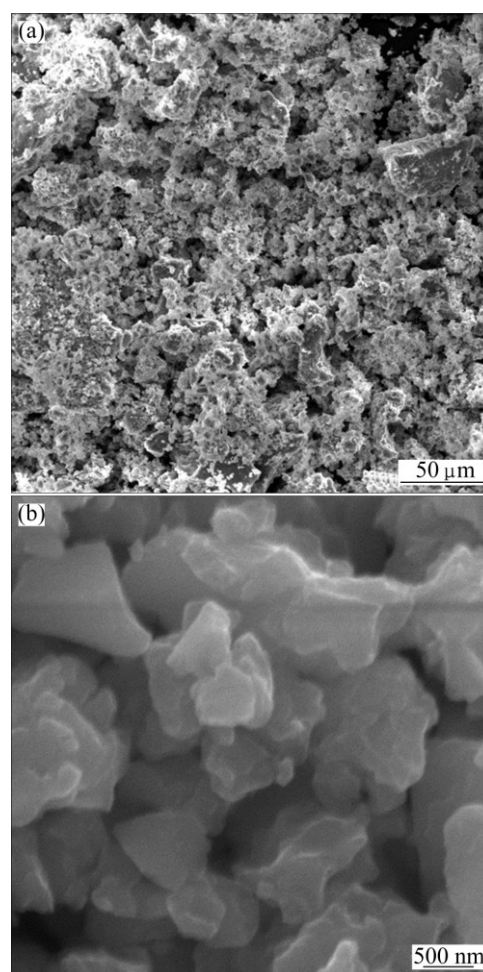


Fig. 3 Microstructures of MgNi26 alloy prepared by MA: (a) Lower magnification; (b) Higher magnification

observation confirms that fine nanostructured particles are obtained after mechanical alloying.

The fine nano-structure of ribbons was produced by the rapid solidification of the MgNi26 alloy (Fig. 6). However, the composition does not correspond to the constitution phase diagram of Mg–Ni [9] (see Fig. 7). In Fig. 6, the dark rounded particles correspond to the disequilibrium phase of Mg_6Ni , while the light regions correspond to α -Mg.

3.2 Hydrogen content

3.2.1 As-cast MgNi26

The hydrogen content profile obtained by the GDS analysis of the MgNi26-GC sample after electrochemical hydriding is presented in Fig. 8. It could be observed that the MgNi26-GC sample achieved a maximum hydrogen content of nearly 1.6% on the surface, and the maximum penetration depth of hydrogen was approximately 120 μm . Based on the shape of the hydrogen profile in Fig. 8, the behavior of MgNi26-GC sample during hydriding could be deduced. The hydrogen profile shows

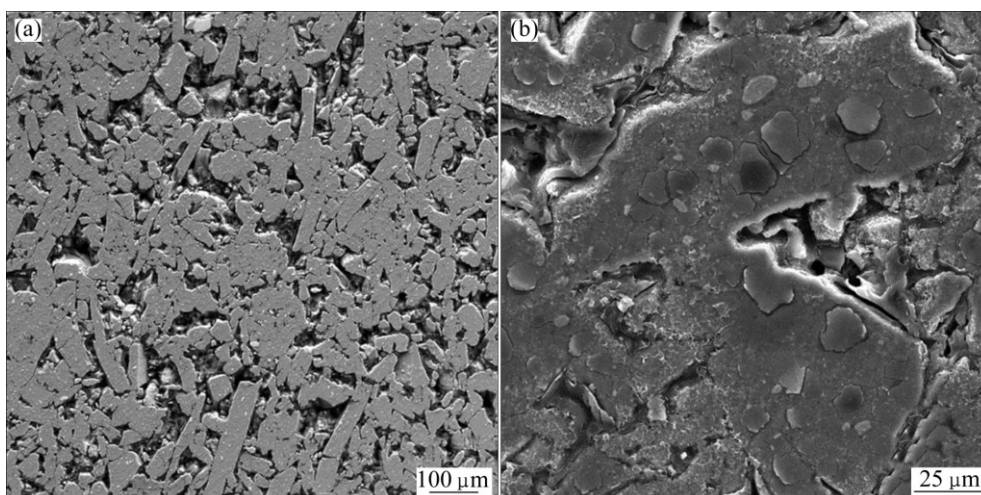


Fig. 4 Microstructures of section of cold-pressed MgNi26-MA sample: (a) Lower magnification; (b) Higher magnification

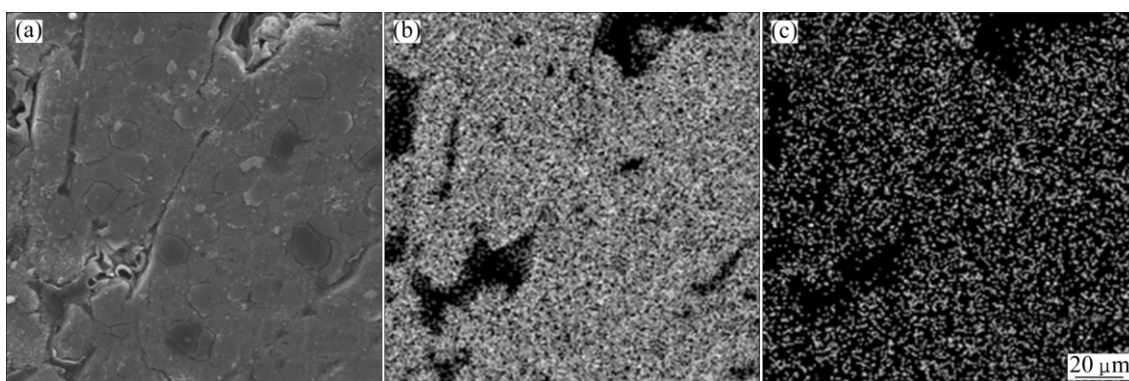


Fig. 5 X-ray elemental maps of cold-pressed MgNi26-MA sample: (a) SEM image; (b) Mg; (c) Ni

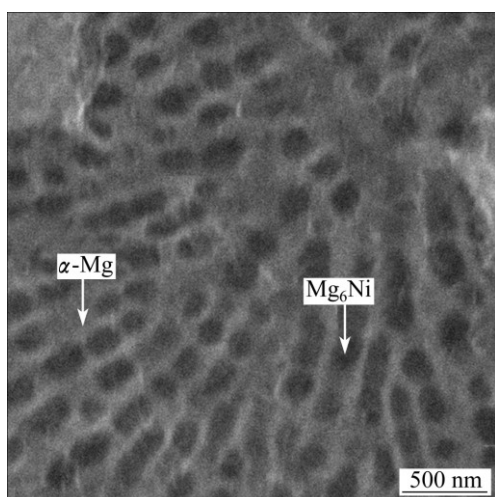


Fig. 6 Microstructure of MgNi26-RS sample

a typical diffusion shape, in which the hydrogen content progressively decreases from the surface to the alloy interior. Although the decrease in the hydrogen content is very rapid (1/8 of the maximum surface content in half of the penetration depth), the depth of hydrogen detection is quite high. This phenomenon may be attributed to the fine eutectic structure, where diffusion through the interphase boundaries could occur much

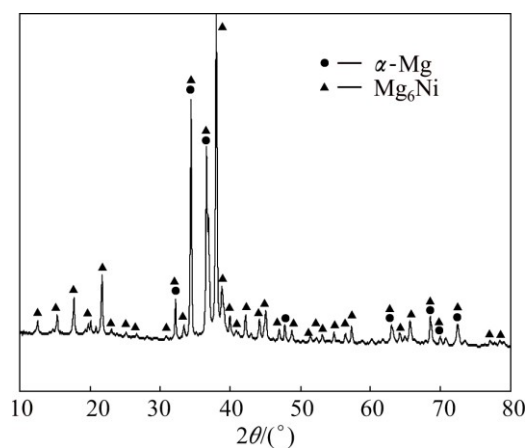


Fig. 7 XRD pattern of MgNi26-RS sample

more readily than that in bulk phase. Indeed, to obtain a few micrometers of MgH₂ on the surface of bulk Mg requires longer time of gas hydriding at high temperatures [10]. This is caused by much lower diffusion coefficient of hydrogen in MgH₂ compared with that in Mg [11]. Once the layer of MgH₂ is created, further hydrogen diffusion is practically stopped. From this point of view, the fine structure with conduits for rapid hydrogen diffusion is necessary to obtain a high

content of absorbed hydrogen. The maximum hydrogen content of 1.6% achieved by the MgNi26-GC sample is seemingly low, but the mild condition of hydriding and the as-cast state of the sample should be taken into account.

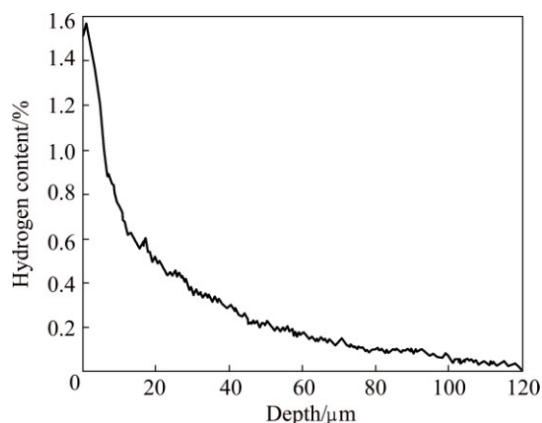


Fig. 8 Hydrogen content profile after electrochemical hydriding for GC sample (GDS)

3.2.2 Powdered and rapidly solidified samples

The powder of mechanically alloyed MgNi26 alloy (MgNi26-MA) was pressed into a pellet (1 mm in length) and electrochemically hydrided. The ribbons (60 μm in length) of MgNi26 obtained by rapid solidification (MgNi26-RS) were electrochemically hydrided without any treatment. The total hydrogen contents achieved after the electrochemical hydriding of the powdered and rapidly solidified samples are summarized in Fig. 9. The total amount of hydrogen absorbed by the MgNi26-GC, calculated as an integration of the hydrogen profile (see Fig. 8) for a 1 mm-thick sample, is also included in Fig. 9. For the conversion of a 1 mm-thick sample in the case of MgNi26-GC, the density $\rho=2.23 \text{ g/cm}^3$ obtained by the Archimedes method was used.

The comparison of the maximum hydrogen content for MgNi26-GC (see Fig. 8) and MgNi26-MA (see Fig. 9) slightly favors the former. However, the hydrogen content in the MgNi26-MA sample is the average

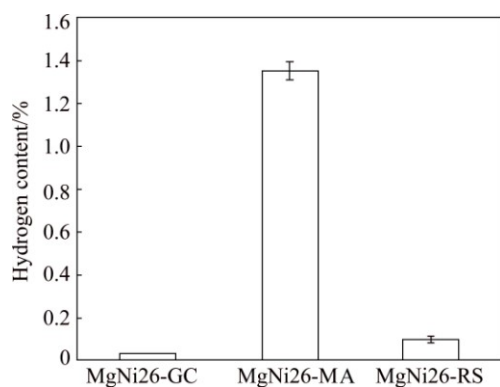
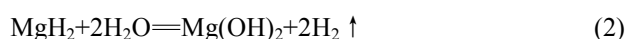
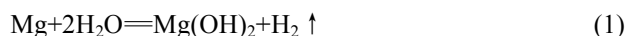


Fig. 9 Hydrogen contents of gravity-cast (GC), mechanically alloyed (MA) and rapidly solidified (RS) samples of MgNi26 alloy after hydriding (Hydrogen content in MgNi26-GC corresponds to 1 mm-thick sample)

amount for a 1 mm-thick sample. Therefore, the real amount of absorbed hydrogen is much higher for the mechanically alloyed sample than that for the gravity cast one. This is evident in Fig. 9. The hydrogen content in the MgNi26-MA sample is approximately 30 times higher than that in the MgNi26-GC sample. This means that mechanical alloying is beneficial to obtaining a high amount of absorbed hydrogen. The high deformation of the metal powders during the mechanical alloying results in both many lattice defects in the formed phases and fine nanostructured grains. That structure fulfils demand for high velocity trapping, diffusion and reaction of atomic hydrogen within the material during electrochemical hydriding. We assume that the microstructure of MgNi26-MA alloy is not affected by cold pressing, so the properties are equal to those of unpressed powder. Moreover, the pellet obtained is suitable for electrochemical hydriding and the high porosity obtained supports the easy access of atomic hydrogen to the interior material.

The milling time of the MgNi26-MA alloy was 8 h. A longer time could probably provide better results due to the refining of the Mg and Mg₂Ni particles. On the other hand, finer particles of Mg are susceptible to the oxidation and formation of Mg(OH)₂ during electrochemical hydriding. Mg(OH)₂ can be formed by the reaction of Mg or MgH₂ with water, according to Reactions (1) or (2), respectively. Reaction (2) runs slowly at room temperature but is rather fast in hot water.



The layer of Mg(OH)₂ inhibits further hydrogen diffusion. Moreover, it serves as an insulant that reduces an access of charge and suspects hydrogen evolution. Finally, the electrochemical hydriding of Mg nanoparticles could lead to poor results for absorbed hydrogen because it is hard to protect Mg against Mg(OH)₂ formation.

Although some recent studies show excellent hydrogen characteristics of rapidly solidified Mg–Ni-based alloys [12,13], the MgNi26-RS sample absorbs a negligible amount of hydrogen compared to the MgNi26-MA sample (Fig. 9). There are at least two probable reasons for this poor hydrogen absorption. The first reason is the just mentioned rapid oxidation of the nano-crystalline Mg present in the structure (see Fig. 6). The second reason is the presence of the non-equilibrium Mg₆Ni phase, which is not able to absorb hydrogen or serve as a catalyst for hydrogen absorption [14].

3.3 Phase composition after hydriding

After the electrochemical hydriding of the samples, XRD analyses were performed. The result of this

analysis for MgNi26-MA (Fig. 10) shows that the main hydriding product is MgH₂.

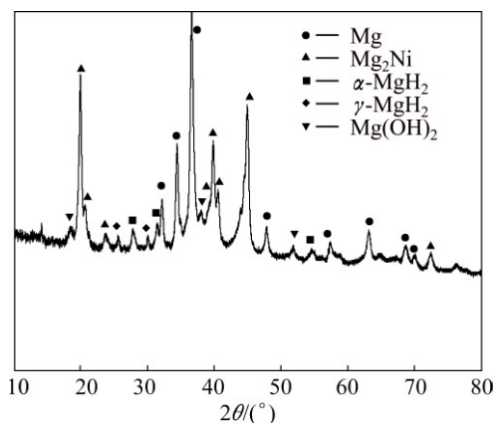


Fig. 10 XRD pattern of MgNi26-MA sample after electrochemical hydriding

It is surprising to find that no ternary Mg₂NiH₄ hydride is observed. This ternary hydride is often detected after hydriding in gaseous hydrogen at high temperatures and pressures. Although Mg₂NiH₄ hydride shows better thermodynamics of decomposition compared to MgH₂, the formation of MgH₂ occurs before the Mg₂NiH₄ formation during gas hydriding [15]. In the case of the Mg₂NiH₄ phase, the explanation of why this ternary hydride was not formed in this study might be the large energy barrier of transformation of Mg₂NiH_{0.3} to Mg₂NiH₄. This energy barrier is caused by the large differences in the lattice parameters of these phases. The Mg₂NiH_{0.3} phase is characterized by the *P*₆₂₂ space group with lattice parameters of *a*=0.525 nm and *c*=1.343 nm [16], whereas the low temperature Mg₂NiH₄ hydride has the *C*2/*c* space group with parameters of *a*=1.434 nm, *b*=0.640 nm and *c*=0.648 nm [17]. The temperature used for electrochemical hydriding is most likely not sufficient to overcome this energy barrier to form the Mg₂NiH₄ hydride. Alternatively, the MgH₂ hydride has a tetragonal lattice (*P*42/*mnm* space group) with unit cell parameters of *a*=0.452 nm and *c*=0.302 nm [18]. By comparing these parameters with those of α-Mg (hexagonal *P*63/*mmc* space group with parameters of *a*=0.324 nm and *c*=0.526 nm [18]), it can be assumed that the transformation from Mg to MgH₂ proceeds more readily and faster than the formation of Mg₂NiH₄ from Mg₂NiH_{0.3}.

Two polymorphic modifications of MgH₂, namely, α-MgH₂ and γ-MgH₂ were detected in the hydrided MgNi26-MA sample (Fig. 10). The transition from α-MgH₂ to γ-MgH₂ can be fully achieved by high pressure treatment and partially by the intensive ball milling of α-MgH₂ [19]. In this work, we showed that γ-MgH₂ can be produced by the hydriding of ball milled magnesium.

3.4 Hydrogen evolution

The hydrogen evolution upon heating was monitored using the temperature-programmed desorption (TPD) technique. Because the XRD analysis detects only the magnesium hydride in these samples, we also subjected pure commercial MgH₂ powder to TPD analysis for comparison. The results from the TPD analyses of the hydrided alloys and commercial MgH₂ are shown in Fig. 11.

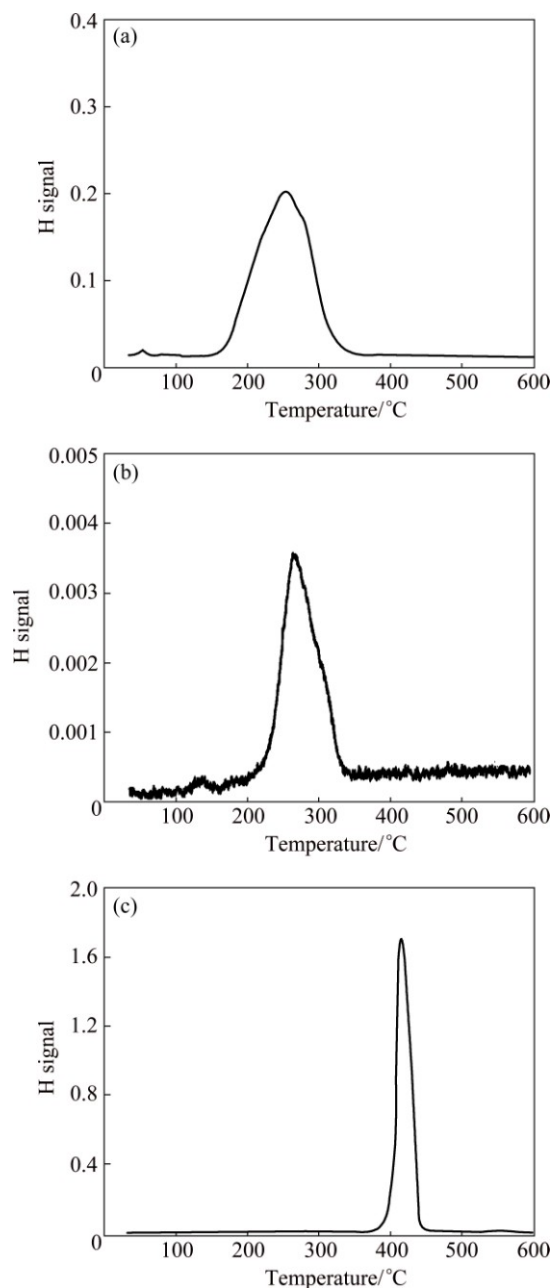


Fig. 11 Dehydriding curves of MgNi26-MA (a), MgNi26-RS (b) and commercial MgH₂ (c) powders obtained by TPD

From the hydrogen peaks of desorption that were obtained by the TPD analyses (Fig. 11), the temperatures of the start, maximum and end of the hydrogen evolution can be determined for each alloy. These temperatures,

including the results for the pure MgH_2 powder, are given in Table 1.

Table 1 Temperatures of start, maximum and end of each hydrogen peak obtained by TPD analyses of hydrided samples and pure MgH_2 powder

Sample	Start temperature of hydrogen peak/°C	Maximum temperature of hydrogen peak/°C	End temperature of hydrogen peak/°C
MgNi26-MA	170	268	322
MgNi26-RS	208	273	320
MgH_2	376	414	463

The MgNi26-MA sample shows a broad peak (Fig. 11(a)) of hydrogen evolution, most likely due to the presence of two polymorphic MgH_2 modifications, namely α - MgH_2 and γ - MgH_2 . The shape of the hydrogen evolution for the MgNi26-MA sample represents the superposition of two peaks, corresponding to the decomposition of α - MgH_2 and γ - MgH_2 . According to the literature, the γ - MgH_2 phase decomposes at a lower temperature [18]. The evolution of hydrogen starts at 170 °C for MgNi26-MA, which is 200 °C lower than that for pure MgH_2 (see Table 1). The presence of the extra-fine crystals of α - MgH_2 and γ - MgH_2 in the hydrided MgNi26-MA sample probably serves as an efficient way to reduce the hydrogen evolution temperature. Indeed, structural refinement is well known to reduce the decomposition temperature of hydrides [20]. In the case of MgNi26-MA dehydriding, the presence of the surrounding Mg_2Ni phase plays a significant role in lowering the hydrogen evolution temperature. The Mg_2Ni phase can serve as a catalyst and active site in hydrogen communication with MgH_2 because the diffusion of hydrogen proceeds faster in the Mg_2Ni phase than in MgH_2 [11].

Because of the small amount of absorbed hydrogen in the MgNi26-RS sample, it was impossible to find out by XRD analysis which type of hydride has been formed. However, based on the results obtained from the TPD analysis (Fig. 11(b)), it could be assumed that only α - MgH_2 is present. The temperature of the start is higher for MgNi26-MA alloy (Fig. 11(a)).

4 Conclusions

1) The surface content of hydrogen in the as-cast MgNi26-GC alloy (1.6%) was very similar to the total amount of absorbed hydrogen in the case of the mechanically alloyed MgNi26-MA alloy (1.3%). However, the comparison of hydrogen content in 1 mm-thick samples shows that the MgNi26-MA alloy

absorbed more than 30 times hydrogen content than the MgNi26-GC alloy. The intensive plastic deformation of the powder during milling probably creates a suitable structure for fast and effective electrochemical hydriding.

2) The amount of absorbed hydrogen for the MgNi26-RS alloy was only 0.1% (mass fraction). Against expectations, the utilization of the rapid solidification method of MgNi26 preparation did not bring an improvement in hydrogen absorption by electrochemical hydriding. The reason is most likely the unfavorable phase composition, when the Mg_6Ni phase did not behave in the same manner as Mg_2Ni .

3) The only hydride formed after the electrochemical hydriding was MgH_2 . Compared with pure MgH_2 , the temperature of the hydrogen evolution in the case of the MgNi26-MA alloy was lowered by more than 200 °C. This remarkable decrease was most likely caused by the presence of a fine mixture of MgH_2 and Mg_2Ni crystals and also by the presence of γ - MgH_2 which exhibits a lower decomposition temperature than α - MgH_2 .

Acknowledgments

The authors wish to thank the Czech Science Foundation (project No. P108/12/G043) for the financial support of this research.

References

- [1] BASTIDE J P, BONNETOT B, LÉTOFFÉ J M, CLAUDY P. Polymorphisme of magnesium hydride under high pressure [J]. *Materials Research Bulletin*, 1980, 15: 1779–1787.
- [2] JAIN I P, LAL C, JAIN A. Hydrogen storage in Mg: A most promising material [J]. *International Journal of Hydrogen Energy*, 2010, 35: 5133–5144.
- [3] CHU Hai-liang, QIU Shu-jun, TIAN Qi-feng, SUN Li-xian, ZHANG Yao, XU Fen, LIU Ying-ya, QI Yan-ni, FAN Mei-qiang. Effect of ball-milling time on the electrochemical properties of La-Mg-Ni-based hydrogen storage composite alloys [J]. *International Journal of Hydrogen Energy*, 2007, 32: 4925–4932.
- [4] SPASSOV T, LYUBENOVA L, KÖSTER U, BARÓ M D. Mg-Ni-RE nanocrystalline alloys for hydrogen storage [J]. *Materials Science and Engineering A*, 2004, 375–377: 794–799.
- [5] VOJTĚCH D, MICHALCOVÁ A, KLEMENTOVÁ M, ŠERÁK J, MORŤANIKOVÁ M. Nanocrystalline nickel as a material with high hydrogen storage capacity [J]. *Materials Letters*, 2009, 63: 1074–1076.
- [6] TÖPLER J, BUCHNER H, SÄUFFERER H, KNORR K, PRANDL W. Measurements of the diffusion of hydrogen atoms in magnesium and Mg_2Ni by neutron scattering [J]. *Journal of the Less Common Metals*, 1982, 88: 397–404.
- [7] HA W, LEE H S, YOUN J I, HONG T W, KIM Y J. Hydrogenation and degradation of Mg-10%Ni alloy after cyclic hydriding-dehydriding [J]. *International Journal of Hydrogen Energy*, 2007, 32: 1885–1889.
- [8] KNOTEK V, VOJTĚCH D. Electrochemical hydriding performance of Mg-TM-Mm (TM=transition metals, Mm=mischmetal) alloys for hydrogen storage [J]. *Transactions of Nonferrous Metals Society of China*, 2013, 23: 2047–2059.

- [9] GALE W F, TOTEMEIER T C. Smithells metals reference book [M]. 8th ed. Amsterdam: Elsevier, 2004.
- [10] LIU Wei-hong. The electrolyte temperature dependence of the electrochemical hydrogen storage property of Mg–Ni alloy codeposited from aqueous solution [J]. *Journal of Alloys and Compounds*, 2005, 404–406: 694–698.
- [11] ČERMÁK J, KRÁL L. Hydrogen diffusion in Mg–H and Mg–Ni–H alloys [J]. *Acta Materialia*, 2008, 56: 2677–2686.
- [12] ZHANG Yang-huan, XU Sheng, ZHAI Ting-ting, YANG Tai, YUAN Ze-ming, ZHAO Dong-liang. Hydrogen storage kinetics of nanocrystalline and amorphous Cu–Nd-added Mg₂Ni-type alloys [J]. *Transactions of Nonferrous Metals Society of China*, 2014, 24: 3524–3533.
- [13] ZHANG Yang-huan, HAN Zhong-gang, YUAN Ze-ming, YANG Tai, QI Yan, ZHAO Dong-liang. Electrochemical properties of nanocrystalline and amorphous Mg–Y–Ni alloys applied to Ni–MH battery [J]. *Transactions of Nonferrous Metals Society of China*, 2015, 25: 3736–3746.
- [14] SPASSOV T, KÖSTER U. Hydrogenation of amorphous and nanocrystalline Mg-based alloys [J]. *Journal of Alloys and Compounds*, 1999, 287: 243–250.
- [15] DAVID E. An overview of advanced materials for hydrogen storage [J]. *Journal of Materials Processing Technology*, 2005, 162–163: 169–177.
- [16] MASSALSKI T B, OKAMOTO H, SUBRAMANIAN P, KACPRZAK L. Binary alloy phase diagrams [M]. 2nd ed. Ohio: ASM International, 1990.
- [17] ZHANG J, ZHOU D W, HE L P, PENG P, LIU J S. First-principles investigation of Mg₂Ni phase and high/low temperature Mg₂NiH₄ complex hydrides [J]. *Journal of Physics and Chemistry of Solids*, 2009, 70: 32–39.
- [18] DENYS R V, RIABOV A B, MAEHLER J P, LOTOTSKY M V, SOLBERG J K, YARTYS V A. In situ synchrotron X-ray diffraction studies of hydrogen desorption and absorption properties of Mg and Mg–Mm–Ni after reactive ball milling in hydrogen [J]. *Acta Materialia*, 2009, 57: 3989–4000.
- [19] VARIN R A, CZUJKO T, WRONSKI Z. Particle size, grain size and γ -MgH₂ effects on the desorption properties of nanocrystalline commercial magnesium hydride processed by controlled mechanical milling [J]. *Nanotechnology*, 2006, 17: 3856–3865.
- [20] NIEMANN M U, SRINIVASAN S S, PHANI A R, KUMAR A, GOSWAMI D Y, STEFANAKOS E K. Nanomaterials for hydrogen storage applications: A review [J]. *Journal of Nanomaterials*, 2008, 2008: 1–9.

纳米结构贮氢合金 MgNi₂₆ 的电化学氢化和热脱氢性能

V. KNOTEK¹, O. EKRT¹, M. LHOTKA², D. VOJTĚCH¹

1. Department of Metals and Corrosion Engineering, University of Chemistry and Technology Prague,
Technická 5, 166 28 Prague 6, Czech Republic;
2. Department of Inorganic Technology, University of Chemistry and Technology Prague,
Technická 5, 166 28 Prague 6, Czech Republic

摘要: 采用重力铸造(GC)、机械合金化(MA)和快速凝固(RS) 3 种工艺制备 MgNi₂₆ 合金。将所有样品在浓度为 6 mol/L 的 KOH 溶液中于 80 °C 进行电化学氢化处理 240 min。采用光学显微镜、扫描电镜、能量分散光谱及 X 射线衍射技术研究合金的组织 and 相组成。利用程序控温技术分析吸氢和脱氢过程。机械合金化法制备的 MgNi₂₆-MA 合金样品所吸附的氢含量(约 1.3%, 质量分数)比重力铸造法制备的 MgNi₂₆-GC 合金样品所吸附的氢含量高 30 倍。快速凝固法制备的 MgNi₂₆-RS 合金样品所吸附的氢含量仅为 0.1%。MgNi₂₆-MA 合金显示出最低的析氢温度。与工业纯 MgH₂ 相比, MgNi₂₆-MA 合金的分解温度至少降低了 200 °C。MgNi₂₆-MA 合金优异的氢化和脱氢性能归因于其有利的相组成和组织结构。

关键词: 镁合金; 贮氢; 电化学氢化; 机械合金化; 熔融纺丝法

(Edited by Wei-ping CHEN)